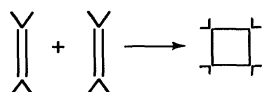


tine and phototransformed  $C_{60}$  films, which were obtained with 488-nm excitation, suggest a similar conclusion (27). The strongest peak in pristine  $C_{60}$ , which was at  $\sim 725$  nm, redshifted  $\sim 20$  nm on phototransformation. The small changes in these electronic spectra are consistent with the polymerization of fullerene molecules.

Finally, the phototransformation of solid  $C_{60}$  altered x-ray diffraction of the films. Using Cu  $K_{\alpha}$  x-rays, we observed three clear peaks in  $\sim 5000$  Å-thick pristine films that could be indexed according to the fcc lattice: (111), (220), and (311). Phototransformation broadened these peaks by  $\sim 20\%$ , which indicates an increase in disorder in the film, and the peaks shifted slightly to higher scattering angles, which is expected for an average contraction of  $\sim 0.1$  Å in the lattice constant. This contraction is much less than one might expect for a simple polymerization of  $C_{60}$  units in which the van der Waals bond between  $C_{60}$  molecules ( $\sim 3.0$  Å) is replaced by a covalent C–C bond ( $\sim 1.5$  Å). This could occur, for example, if a 2 + 2 cyclo addition photochemical reaction (28) were to take place. In the case of adjacent  $C_{60}$  molecules, parallel double bonds (C=C), one from each molecule, are broken and reform as single bonds between the molecules, that is



which results in a 1.5 Å contraction in the bond between the molecules, which would appear to be inconsistent with our preliminary x-ray results. However, the phototransformation may involve the conversion of  $(C_{60})(C_{60}) \rightarrow C_{60}=C=C=C_{58}$ —that is, the formation of a (=C=C=) bridge, which preserves the  $\sim 10$  Å center-to-center distance between adjacent fullerenes. Further work will be necessary to determine the nature of the photoinduced intermolecular coupling.

*Note added in proof:* Our recent Raman scattering studies of  $C_{60}$  in the range 30 to 200  $cm^{-1}$  clearly indicate that phototransformation introduces a new mode at  $\omega \sim 116$   $cm^{-1}$ , which we identify with an intermolecular vibrational mode. Furthermore, intercalated  $O_2$  has been found in other Raman scattering studies (12) to harden the  $C_{60}$  films against phototransformation. Because  $O_2$  also quenches the luminescence of the first excited triplet state of  $C_{60}$  (27), it appears that the nearly 100% efficient transition from the singlet manifold to this triplet state and the reactivity of the molecule in this triplet state are both important to efficiently produce the polymerized form of  $C_{60}$ .

## REFERENCES AND NOTES

- H. W. Kroto, J. R. Heath, S. C. O'Brien, R. F. Curl, R. E. Smalley, *Nature* **318**, 162 (1985).
- H. Kroto, *Science* **242**, 1139 (1988).
- R. F. Curl and R. E. Smalley, *ibid.*, p. 1017.
- For recent reviews of fullerene-based solids, see the special issue of *Acc. Chem. Res.* **25**, 98 (1992).
- M. S. Dresselhaus, G. Dresselhaus, P. C. Eklund, in preparation.
- P. A. Heiney *et al.*, *Phys. Rev. Lett.* **66**, 2911 (1991).
- P. A. Heiney *et al.*, *ibid.* **67**, 1468 (1991).
- C. S. Yannoni, R. D. Johnson, G. Meijer, D. S. Bethune, J. R. Salem, *J. Phys. Chem.* **95**, 9 (1991).
- R. Tycko *et al.*, *Phys. Rev. Lett.* **68**, 1912 (1992).
- D. Loy and R. Assink, *J. Am. Chem. Soc.* **114**, 3977 (1992).
- Y. Wang, *Nature* **356**, 585 (1992).
- P. Zhou *et al.*, *Appl. Phys. Lett.* **60**, 2871 (1992).
- P. C. Eklund, P. Zhou, K.-A. Wang, G. Dresselhaus, M. S. Dresselhaus, *J. Phys. Chem. Solids* **53**, 1391 (1992).
- S. J. Duclos, R. C. Haddon, S. H. Glarum, K. B. Lyons, *Solid State Commun.* **80**, 481 (1991).
- K. Sinha, S. Guha, J. Menendez, D. A. Wright, T. Karcher, *Phys. Rev. B*, in press.
- B. Chase, N. Herron, E. Holler, *J. Phys. Chem.* **96**, 4262 (1992).
- Y. Wang *et al.*, *Phys. Rev. B* **45**, 14396 (1992).
- A. M. Rao *et al.*, in preparation.
- P. H. M. van Loosdrecht, P. J. M. van Bentum, G. Meijer, *Europhys. Lett.*, in press.
- D. S. Cornett, I. J. Amster, M. A. Duncan, A. M. Rao, P. C. Eklund, in preparation.
- C. Yeretizian, K. Hansen, F. Diederich, R. L. Whetten, *Nature* **359**, 44 (1992).
- G. Meijer and D. S. Bethune, *Chem. Phys. Lett.* **175**, 1 (1990).
- G. Dresselhaus, M. S. Dresselhaus, P. C. Eklund, *Phys. Rev. B*, in press.
- P. J. Fagan, J. C. Calabrese, B. Malone, *Acc. Chem. Res.* **25**, 134 (1992).
- B. Chase and P. J. Fagan, *J. Am. Chem. Soc.* **114**, 2252 (1992).
- K.-A. Wang *et al.*, *Phys. Rev. B* **45**, 1955 (1992).
- Y. Wang *et al.*, in preparation.
- J. D. Coyle, *Introduction to Organic Photochemistry* (Wiley, New York, 1986), p. 61.
- This work was funded, in part, by the University of Kentucky Center for Applied Energy Research and, at the University of Georgia, by NSF grants CHEM-9008246 (M.A.D.) and CHE-9024992 (I.J.A.). We thank A. W. Overhauser (Purdue University) for discussions on the possibility of photoinduced polymerization. Discussions with K. R. Subbaswamy (University of Kentucky), F. Zerbetto (Bologna University), and M. S. Dresselhaus and G. Dresselhaus (Massachusetts Institute of Technology) are also gratefully acknowledged.

24 September 1992; accepted 30 November 1992

## Electrochemical Processing of Conducting Polymer Fibers

Shulong Li, Christopher W. Macosko, Henry S. White\*

An electrochemical method for growing macroscopic fibers of electrically conductive poly(3-methylthiophene) is described. Single fibers of uniform diameter ( $\sim 0.1$  to 0.7 millimeter) and length greater than 10 centimeters are grown in a capillary flow cell by electrochemical oxidation of the monomer, 3-methylthiophene. The shapes and diameters of the resulting fibers are determined by the fluid flow pattern in the cell. Straight fibers, sawtooth-shaped fibers, and fibers with tapered necks can be grown by varying the capillary shape.

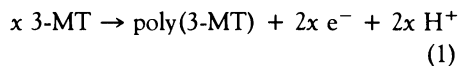
The high electrical conductivity of heteroaromatic polymers, such as polythiophene, polypyrrole, and polyaniline, has spurred interest in the use of these materials in novel electronic and chemical applications (1, 2). Prototype designs of flexible light-emitting diodes (3), molecular transistors (4), lightweight battery electrodes (5), electrochromic displays (6), and anticorrosion films (7) in which a conductive polymer is the active element have been realized during the past decade. However, most electrically conductive polymers are insoluble or intractable or decompose before melting, which prevents the use of conventional polymer-processing techniques in shaping these materials into desired structures.

Several methods for processing conductive polymer fibers require multistep chemical or mechanical procedures (8–12). In this report, we describe a one-step electrochemical process for synthesizing macroscopic electrically conductive fibers of poly(3-methylthiophene) [poly(3-MT)]. Conductive poly(3-MT) fibers were grown in a two-electrode flow cell, shown in Fig. 1. The main body of the cell consists of a glass capillary 3 mm in inner diameter, oriented vertically. The electrolyte solution containing the monomer, 3-methylthiophene (3-MT) (13), is pumped through the cell with a centrifugal pump. Polymer fibers are grown from a Pt wire 127  $\mu m$  in diameter, which is encapsulated in glass with  $\sim 1$  cm of the wire extending past the end of the glass insulation. This electrode is positioned in the center of the capillary  $\sim 5$  cm from the entrance port to reduce the effects of entrance flow. A second Pt wire 1 mm in diameter and  $\sim 2$  cm long, is positioned at the bottom of the tube near the exit port. The

Department of Chemical Engineering and Materials Science, University of Minnesota, Minneapolis, MN 55455.

\*To whom correspondence should be addressed.

monomer is oxidized at the upper Pt wire by the passage of a constant anodic current through the cell (14):



Continuous flow of current through the cell results in the growth of a single, conductive poly(3-MT) fiber attached to the end of the electrode.

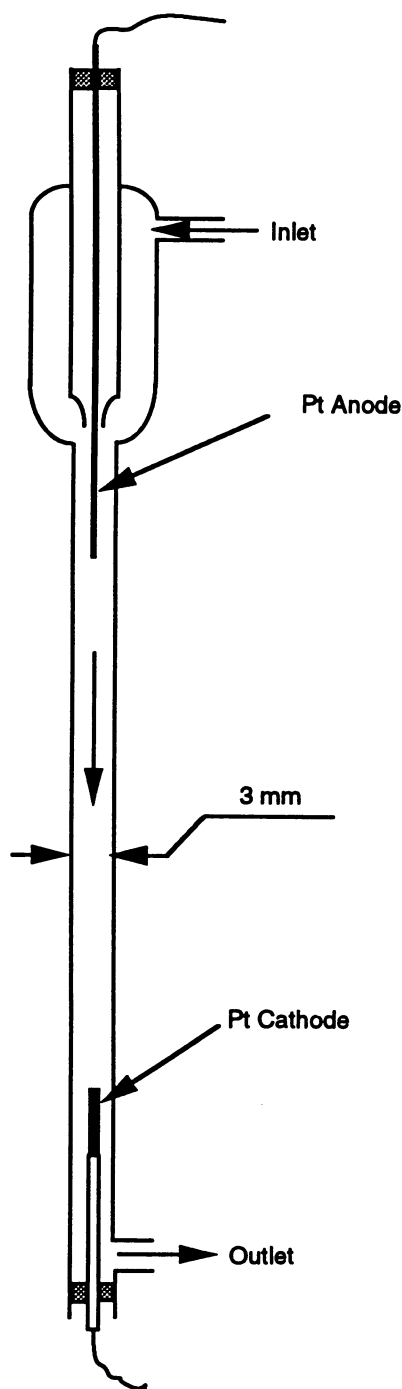


**Fig. 1.** Schematic drawing of the electrochemical flow cell used to grow conducting poly(3-MT) fibers. A centrifugal pump is used to pump the electrolyte solution through the cell.

An optical photograph of a portion of a poly(3-MT) fiber ~11 cm long and 0.6 mm in diameter grown over a period of ~14 hours is shown in Fig. 2A. The fiber was grown at a constant current of 1.8 mA in a flowing acetonitrile solution ( $2 \text{ ml s}^{-1}$ ) containing 0.5 M 3-MT and 0.1 M tetrabutylammonium perchlorate (TBAP) as the supporting electrolyte. The length of the fiber increased at a constant rate of  $\sim 0.8 \text{ cm hour}^{-1}$  and was limited only by the length of the electrochemical cell. The fiber diameter is uniform and is controlled by the diameter of the capillary in which it is synthesized, decreasing in cells of smaller diameter. A concentric sheath of the electrolyte containing the monomer flows between the fiber and the cell walls, transporting monomer to the tip of the fiber where it is attached, according to Eq. 1, to the growing fiber.

The current efficiency [that is, the current consumed by the growth of the poly(3-MT) fiber relative to the total current passed in the cell] was estimated from Eq. 2:

$$\text{current efficiency} = nFv\rho A/(iMW) \times 100 \quad (2)$$

where  $F$  is the Faraday constant ( $96,485 \text{ C/eq}$ ),  $v$  is the linear rate of fiber growth (in centimeters per second),  $\rho$  is the polymer density ( $\sim 1 \text{ g cm}^{-3}$ ),  $A$  is the cross-sectional area of the fiber (in centimeters),  $MW$  is the molecular weight of 3-(MT),  $i$  is the applied current (in amperes), and  $n$  is the number of electrons transferred per monomer attached to the polymer. From Eq. 1,  $n = 2$ . However, under the electrochemical conditions used here, the resulting polymer is further oxidized to the charged and conducting state [ $\text{poly(3-MT)} \rightarrow \text{poly(3-MT)}^{\delta+}$ , where  $\delta$  is reported to be  $\sim 0.25$  per

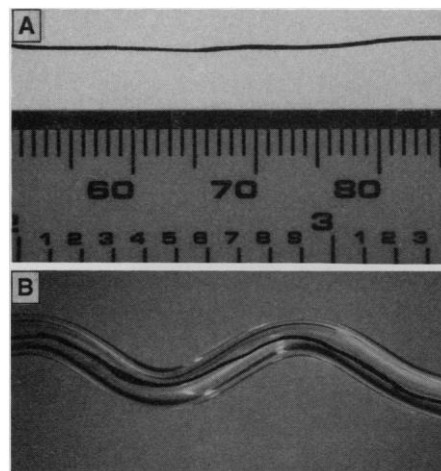


**Fig. 2.** Optical photographs of conducting poly(3-MT) fibers. (A) A straight fiber prepared in the electrochemical flow cell shown in Fig. 1. The total length of the fiber is 11 cm. (B) A zigzag fiber grown in a zigzag tube.

monomer unit (15)]. Thus, if we use  $n = 2.25$ , the current efficiency for fiber synthesis is  $80 \pm 15\%$ .

Poly(3-MT) fibers of various arbitrary shapes can be synthesized if the cell geometry is varied. A sawtooth-shaped polymer fiber is produced in a sawtooth-shaped cell tube (Fig. 2B). As with the growth of straight fibers, the zigzag-shaped fiber does not touch the walls of the cell, which demonstrates that the electrolyte flow pattern controls the growth direction of the fiber. The fiber diameter can also be changed if the cell tube diameter is varied. We have used this finding to produce tapered fibers (both increasing and decreasing diameter) in tapered cell bodies. This observation also indicates that monomer attachment occurs at the tip of the fiber where the direction of fiber growth is affected by local fluid flow. Only a straight fiber would be obtained if the monomer attachment occurred at the fiber base. In one experiment, we allowed the fiber to grow close to the cathode positioned at the bot-

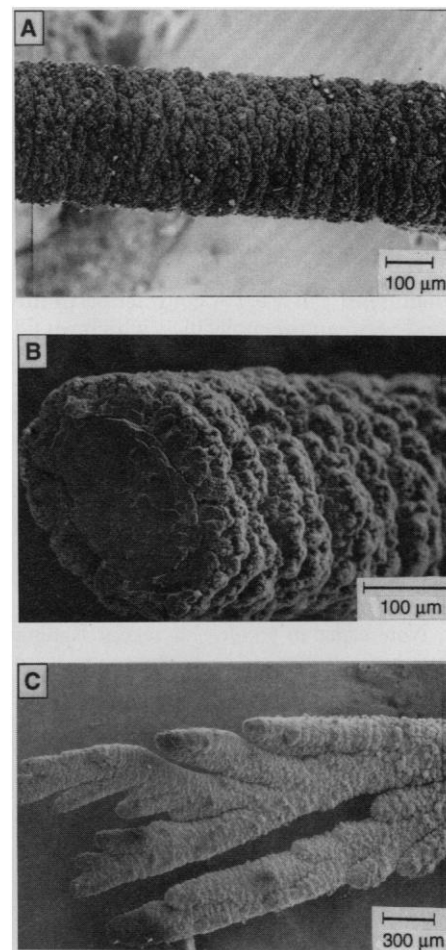


**Fig. 3.** SEM images of the poly(3-MT) fibers. (A) Side view of the fiber surface; (B) the fracture cross section; and (C) a poly(3-MT) fiber grown at a high current (5 mA), showing dendritic growth.

tom of the cell. As the fiber grew to within  $\sim 1$  mm of the tip of the cathode, the direction of growth changed to allow the fiber to grow in the annulus between the cathode and the cell wall. This observation demonstrates that the current distribution has an insignificant effect on the direction of fiber growth.

The conductivity of air-dried poly(3-MT) fibers, measured by the four-point probe method along the length of a 1-cm-long fiber, was  $\sim 20$  ( $\text{ohm cm}^{-1}$ ). This value is comparable to the reported conductivity [ $10$  to  $30$  ( $\text{ohm cm}^{-1}$ )] of poly(3-MT) thin films (15). X-ray diffraction patterns of poly(3-MT) displayed a weak single diffraction ring after a 4-hour exposure, indicating that the fiber has very small crystallinity and that alignment of polymer chains within the fiber is negligible.

Scanning electron microscopy (SEM) images of poly(3-MT) fibers (Fig. 3, A through C) show that the fibers have a rough porous surface and a dense core. (We have observed that hollow fibers are occasionally synthesized by the procedure described above. We speculate that the presence or absence of a hollow center is associated with phenomena that are occurring during nucleation of the fiber, albeit for reasons yet not understood.) The poly(3-MT) fibers fracture easily with handling and are brittle, as indicated by the smooth fracture cross section shown in the SEM micrograph (Fig. 3B). We have not attempted to quantitatively measure the mechanical properties. However, we have tried to improve the mechanical properties of the fiber by the incorporation of polymer electrolytes. For example, we have incorporated poly(styrenesulfonate) (PSS, MW = 70,000) into the poly(3-MT) fiber by adding PPN-PSS [1% by weight; PPN stands for bis(triphenylphosphoanylidene)ammonium cation] to the electrolyte solution. The resulting fiber is significantly stronger than poly(3-MT) fibers grown without PSS and can be handled without fracturing. Detailed studies of this and other composite fibers will be described elsewhere (16).

We tested the electrochemical activity

of a poly(3-MT) fiber by cyclic voltammetry in a stagnant acetonitrile solution containing only supporting electrolyte (0.1 M TBAP). In this experiment, a copper wire was epoxied to the end of a 1-cm length of a poly(3-MT) fiber. The fiber was then immersed in the electrolytic solution and used as the working electrode in a conventional three-electrode cell. The polymer fiber was oxidized beginning at  $\sim 0.8$  V versus the saturated calomel reference electrode (SCE), as indicated by the onset of a large monotonically increasing anodic current at this potential (no anodic peak was observed up to 3 V versus SCE). A cathodic wave centered at 0.2 V versus SCE was observed on the reverse scan ( $2 \text{ mV s}^{-1}$ ), corresponding to the rereduction of the oxidized fiber.

Several experimental parameters (flow rate, faradaic current, and monomer concentration) have a pronounced effect on the shape and quality of the resulting fiber. Fiber growth does not occur in stagnant solutions; in such solutions a smooth thin film or a rough, porous powdery deposit is obtained on the upper Pt electrode, in agreement with previous reports of poly(3-MT) thin film deposition (15, 17). An average flow rate of  $10 \text{ cm s}^{-1}$  [corresponding to a Reynold's number (18) of 700] is required to grow a conducting polymer fiber in the 3-mm-diameter flow cell. Fibers can be grown at flow rates that correspond to laminar and turbulent conditions (Reynolds number between 700 and  $\sim 10^4$ ). Figure 4 shows the dependence of the linear growth rate and the diameter of fibers on the fluid velocity in the capillary flow cell. Although the growth rate decreases linearly with increasing fluid velocity for velocities between 10 and  $60 \text{ cm s}^{-1}$ , the fiber diameter increases only by a factor of  $\sim 2$ . As a result of the offsetting dependencies of the linear growth rate and diameter, the net volumetric growth rate ( $\sim 5 \times 10^{-7} \text{ cm}^3 \text{ s}^{-1}$ ) remains essentially constant over the range of flow rates studied. Thus, the current efficiency calculated above (80%) is independent of the fluid velocity.

Fibers tend to grow very slowly and with significantly larger diameters when the ap-

plied current is less than 0.8 mA. Smooth fibers with uniform diameters can be reproducibly grown at currents between 1.0 and 3.0 mA. When the current is increased above 3.0 mA, dendritic growth occurs, generating fibers of small diameters as shown in Fig. 3C. Each of the branching fibers continues to grow in the direction of the flow stream.

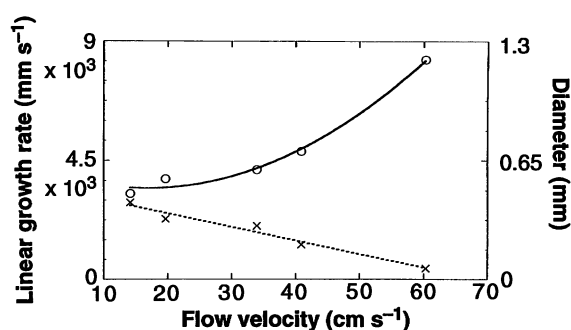
The concentration of 3-MT also plays a key role in the growth of the polymer fiber. Fiber growth does not occur for 3-MT concentrations less than a few millimolar. However, at 3-MT concentrations greater than 2 M, small dendrites form on the surface of the fiber, producing a very porous structure. An intermediate monomer concentration (for example, 0.5 M) is apparently optimal for fiber growth. We have not investigated the influence of the supporting electrolyte concentration and electrolyte resistance beyond placing the counterelectrode at different separation distances from the fiber. This procedure had a very small influence on the growth rate.

Our experimental observations suggest that fiber growth is controlled by coupled transport and reaction processes that are governed by the electrolyte flow patterns in the cell. The mechanism of electrochemical polymerization, proposed initially by Diaz and co-workers for the polymerization of pyrrole (19) and generally accepted by others for the polymerization of 3-MT (1), involves a series of electrochemical and chemical reactions on or near the electrode in which dimeric, trimeric, and oligomeric intermediates are formed and deposited on the surface. It is reasonable to assume that oxidation of 3-MT and subsequent deposition, through oligomer formation, may occur along the sides of the fiber as well as at the fiber tip, because voltammetric experiments in which poly(3-MT) fibers were used as electrodes suggest that the entire surface of the fiber is electrochemically active.

This conclusion appears to contradict our observation that fiber growth occurs only at the fiber tip. We propose that the electrochemical kinetics of 3-MT oxidation or polymer deposition, or both processes, are significantly reduced along the fiber sides, relative to the tip, when the polymer diameter reaches a critical value. This hypothesis is supported indirectly by the abrupt variation in the fiber morphology (Fig. 2B) from a dense core to a very porous outer structure, indicative of a change in the polymerization mechanism or kinetics, or both, at a critical fiber radius.

A similar variation in polymer morphology has been observed during the deposition of thin films of poly(3-MT) in stagnant solution; thin films ( $< 0.1 \mu\text{m}$ ) tend to be smooth and dense, whereas continued

**Fig. 4.** Dependence of the linear growth rate (o) and diameter (x) of poly(3-MT) fibers grown in a straight flow cell 3 mm in diameter. The applied current was 1 mA.



growth results in a porous outer layer (15). Other researchers have correlated the transition in polymer morphology with a decrease in the polymer conductivity (20), although an unambiguous mechanism for the transition has not yet been proposed. However, the similarity between the polymer morphologies of fibers and thin films suggests that the uniformity of the fibers and the high current efficiency result from a decrease in the polymer conductivity in the outer porous layer of the fiber, allowing essentially all of the current to flow to the tip.

The effect of the cell geometry in governing the direction of the fiber growth, demonstrated in Fig. 2, is undoubtedly related to hydrodynamic flow patterns at the tip. The flow of the electrolyte past the fiber tip results in a relatively stagnant fluid layer for which the residence time of chemical intermediates is significantly longer than at the side surface of the fiber. We demonstrated this by inserting a Pt cylindrical electrode 127  $\mu\text{m}$  in diameter in the capillary cell, oriented with its axis perpendicular to the direction of flow. When an anodic current was applied, poly(3-MT) deposition occurred noticeably faster on the back side of the cylindrical electrode than elsewhere, consistent with our hypothesis that the polymer deposition is highest in regions where the residence time of the intermediates is largest. Given this experimental observation, a change in flow direction produced by the cell geometry would tend to orient the direction of the fiber growth in the direction of the flow, consistent with our experimental results. Our results are also consistent with the results of a rotating disk electrode experiment (21), in which a polypyrrole film was deposited preferentially at the center of the rotating disk where the fluid velocity is the smallest.

#### REFERENCES AND NOTES

1. D. Jeon, J. Kim, M. C. Gallagher, R. F. Willis, *Science* **256**, 1662 (1992); J. Heinze, *Top. Curr. Chem.* **152**, 1 (1990); N. C. Billingham and P. D. Calvert, *Adv. Polym. Sci.* **90**, 1 (1989).
2. A. J. Heeger *et al.*, *Synth. Metals* **41-43**, 1027 (1991).
3. J. H. Burroughs *et al.*, *Nature* **347**, 539 (1990); A. J. Heeger *et al.*, *ibid.* **357**, 539 (1992); P. L. Burn *et al.*, *ibid.* **356**, 47 (1992).
4. H. S. White, G. P. Kittlesen, M. S. Wrighton, *J. Am. Chem. Soc.* **106**, 5375 (1984); G. P. Kittlesen, H. S. White, M. S. Wrighton, *ibid.*, p. 7389; D. Bloor, *Nature* **349**, 738 (1991).
5. R. Bittihn *et al.*, *Makromol. Chem. Macromol. Symp.* **8**, 52 (1987); R. J. Mammone and M. Binder, *J. Electrochem. Soc.* **135**, 1057 (1988).
6. C. B. Duke, *Synth. Metals* **21**, 5 (1987); S. Roth, *ibid.*, p. 51; A. G. MacDiarmid, *ibid.*, p. 79.
7. Z. Deng, W. H. Smyrl, H. S. White, *J. Electrochem. Soc.* **136**, 2152 (1989).
8. D. C. Bradley *et al.*, *Synth. Metals* **17**, 473 (1987); J. M. Machado, M. A. Masse, F. E. Karasz, *Polymer* **30**, 1992 (1989).
9. P. Smith *et al.*, *Polymer* **33**, 1102 (1992); M. Ponerantz *et al.*, *Synth. Metals* **41-43**, 825 (1991).
10. A. Andreatta, Y. Cao, J. C. Chiang, A. J. Heeger, P. Smith, *Bull. Am. Phys. Soc.* **34**, 582 (1989); X. Tang, E. Scherr, A. G. MacDiarmid, A. J. Epstein, *ibid.*, p. 583.
11. J. R. Reynolds, M. B. Gieselman, Y.-J. Qiu, M. H. Pyo, *Polym. Mater. Sci. Eng.* **64**, 202 (1991); W. Wernet, *Synth. Metals* **41-43**, 843 (1991); N. Bates, M. Cross, R. Lines, D. Walton, *J. Chem. Soc. Chem. Commun.* **1985**, 871 (1985); L. P. Rector, D. C. De Groot, J. L. Marks, S. H. Carr, *Synth. Metals* **41-43**, 935 (1991).
12. C. R. Martin, Z. Cai, L. S. Van Dyke, W. Liang, *Polym. Mater. Sci. Eng.* **64**, 204 (1991).
13. 3-Methylthiophene (Aldrich) was distilled under ambient pressure. Tetrabutylammonium perchlorate (Kodak) was recrystallized twice in ethyl acetate and dried in vacuum. Acetonitrile (Aldrich) was used as received.
14. A Pine Instrument RDE4 potentiostat-galvanostat was used to supply a constant current to the electrochemical flow cell. The JEOL 840II scanning electron microscope was used to examine the fiber. X-ray diffraction patterns were obtained on a CAD-4 diffractometer.
15. G. Tourillon and F. Garnier, *J. Phys. Chem.* **87**, 2289 (1987).
16. S. Li and H. S. White, in preparation.
17. G. Tourillon and F. Garnier, *J. Polym. Sci. Polym. Phys. Ed.* **22**, 33 (1988).
18. Reynold's number is calculated:  $Re = V_{ave} d_c / \gamma$ , where  $V_{ave}$  is the average flow velocity (in centimeters per second),  $d_c$  is the difference (in centimeters) in the diameters of the cell glass tube and the Pt electrode, and  $\gamma$  is the kinematic viscosity of acetonitrile,  $4.23 \times 10^{-3} \text{ cm}^2 \text{ s}^{-1}$ .
19. E. M. Genies, G. Bidan, A. F. Diaz, *J. Electroanal. Chem.* **149**, 101 (1983).
20. T. F. Otero and E. L. Azelain, *Polymer* **29**, 1522 (1988).
21. P. Lang, F. Chao, M. Costa, F. Garnier, *ibid.* **28**, 668 (1987).
22. This work was supported by the Office of Naval Research and the Center for Interfacial Engineering (NSF Engineering Research Centers Program). We thank D. Britton (University of Minnesota) for the x-ray diffraction analysis.

29 September 1992; accepted 18 December 1992

## Colicin E1 Binding to Membranes: Time-Resolved Studies of Spin-Labeled Mutants

Yeon-Kyun Shin, Cyrus Levinthal, Françoise Levinthal, Wayne L. Hubbell\*

To investigate the mechanism of interaction of the toxin colicin E1 with membranes, three cysteine substitution mutants and the wild type of the channel-forming fragment were spin labeled at the unique thiol. Time-resolved interaction of these labeled proteins with phospholipid vesicles was investigated with stopped-flow electron paramagnetic resonance spectroscopy. The fragment interacts with neutral bilayers at low pH, indicating that the interaction is hydrophobic rather than electrostatic. The interaction occurs in at least two distinct steps: (i) rapid adsorption to the surface; and (ii) slow, rate-limiting insertion of the hydrophobic central helices into the membrane interior.

Colicins are water-soluble cytotoxins secreted by and active against *Escherichia coli* (1). The secreted toxin binds to a receptor in the bacterial outer membrane and is transported into the periplasmic space, where it inserts into the inner membrane to form voltage-sensitive ion channels. Structural domains (receptor binding, translocation, and channel formation) of the protein subserve distinct steps of the cytotoxic process. The functional channel-forming domain of colicin E1, consisting of an  $\sim 20$ -kD COOH-terminal fragment, is readily isolated by trypsinolysis (2). The crystal structure of the analogous fragment of colicin A was recently solved (3, 4); the core of the molecule consists of two extremely hydrophobic  $\alpha$  helices and is surrounded by eight amphipathic  $\alpha$  helices. Two-dimensional nuclear magnetic resonance (NMR) studies (5) generally sup-

port a similar structure for the corresponding colicin E1 fragment. With this information, a structural model of colicin E1 was generated (Fig. 1A) (6).

The channel-forming fragments of colicin A and E1 interact irreversibly with membranes at acidic pH. Although the structure of the membrane-bound form is unknown, the helical content is similar to the soluble form (7), and there is evidence for the insertion of the two core helices into the membrane interior (Fig. 1B) (8). In many ways, the colicin channel-forming fragment is similar to the translocation domain of diphtheria toxin, which consists of nine  $\alpha$  helices, two of which are hydrophobic (9). Membrane insertion and channel formation of diphtheria toxin are triggered by acidic pH. Thus, studies of the colicins may also be germane to the mechanism of action of other toxins.

The recently introduced method of site-directed spin labeling (SDSL) is well suited to time-resolved analysis of structural changes in proteins. In this method, cysteine substitution mutants are used to provide specific attachment sites for nitroxide spin labels. Electron paramagnetic reso-

Y.-K. Shin and W. L. Hubbell, Jules Stein Eye Institute and Department of Chemistry and Biochemistry, University of California, Los Angeles, CA 90024.

C. Levinthal and F. Levinthal, Department of Biological Sciences, Columbia University, New York, NY 10027.

\*To whom correspondence should be addressed.